Solar access of residential rooftops in four California cities

Ronnen Levinson
Hashem Akbari
Melvin Pomerantz
Heat Island Group
Lawrence Berkeley National Laboratory

Smita Gupta
California Energy Commission

March 20, 2009

Abstract

Shadows cast by trees and buildings can limit the solar access of rooftop solar-energy systems, including photovoltaic panels and thermal collectors. This study characterizes residential rooftop shading in Sacramento, San Jose, Los Angeles and San Diego, CA. Our analysis can be used to better estimate power production and/or thermal collection by rooftop solar-energy equipment. It can also be considered when designing programs to plant shade trees.

High-resolution orthophotos and LiDAR (Light Detection And Ranging) measurements of surface height were used to create a digital elevation model of all trees and buildings in a well-treed 2.5 - 4 km^2 residential neighborhood. On-hour shading of roofing planes (the flat elements of roofs) was computed geometrically from the digital elevation model. Values in future years were determined by repeating these calculations after simulating tree growth. Parcel boundaries were used to determine the extent to which roofing planes were shaded by trees and buildings in neighboring parcels.

For the subset of S+SW+W-facing planes on which solar equipment is commonly installed for maximum solar access, absolute light loss in spring, summer and fall peaked about two to four hours after sunrise and about two to four hours before sunset. The fraction of annual insolation lost to shading increased from 0.07 - 0.08 in the year of surface-height measurement to 0.11 - 0.14 after 30 years of tree growth. Only about 10% of this loss results from shading by trees and buildings in neighboring parcels.

1 Introduction

Tree-planting programs designed to shade and cool the south or west sides of buildings can inadvertently limit the solar access of rooftop solar-energy systems, including photovoltaic panels and thermal collectors. Several researchers have modeled the influence of shade on the solar access of buildings. Kaye et al. [1] observed from the street the geometries of the roofs on and trees near 60 houses in an inner-city suburban region of Sydney, Australia. They then used ray-tracing software to predict the locations of on-hour shadows and estimate the average daily output of a nominally 1 kW rooftop photovoltaic array during winter months. Mardaljavec and Rylatt [2] applied the Radiance lighting-simulation system to a three-dimensional model of San Francisco to generate a map of annual insolation on modeled urban surfaces, including walls and roofs. Compagnon [3] also applied Radiance to three-dimensional building models to estimate urban solar availability, but presented results only for walls.

The CH2MHill Solar Automated Feature Extraction^{TM} methodology [4] uses stereo aerial imagery to build three-dimensional model of buildings, then geometrically computes each building's solar access. The current version of this software does not consider trees because it is difficult to determine the heights of curved surfaces from stereo imagery.

Simpson [5] and Akbari [6] each modeled the influence of tree shading on residential energy use for heating and cooling. McPherson and Simpson [7] determined tree-canopy coverage from aerial photographs of 21 California cities to determine the extent to which tree planting programs could reduce energy use in California communities. Akbari et al. [8] and Rose et al. [9] also estimated urban tree cover from high-resolution orthophotos. However, none of these studies quantified shading of rooftops.

This paper estimates the extent to which shading reduces the solar radiation incident on residential roofs in the four California cities of Sacramento, San Jose, Los Angeles and San Diego. This shading analysis can be used to better estimate power production and/or thermal collection by rooftop solar-energy equipment. It can also be considered when designing programs to plant shade trees.

2 Methodology

The locations and elevation profiles of buildings and trees is estimated by combining aerial photography with remote measurements of surface height. The fraction of each flat element of the roof's surface, or "roofing plane," that is shaded at a given hour of the year is determined by geometric computation of the extent to which trees and buildings obscure the path between the sun and the plane. This "shade fraction" gauges only the absence of direct sunlight. It does not distinguish between external shading and self shading and does not measure the absence of global (direct plus diffuse) sunlight.

We calculate two types of shading, "total" and "extraparcel." A plane's total shading is the fraction of its area that is shaded by any surface in the study region. A plane's extraparcel shading is the fraction of its area that is shaded by any surface outside the parcel that contains the plane.

Let "light loss" and "light-loss fraction" denote the absolute and relative reductions in solar access. Since interruption of the solar beam blocks all direct sunlight but little diffuse skylight, we define the plane's light loss (power per unit area) as the product of the shade fraction and the raw direct solar irradiance (power per unit area) that would be received by an unshaded reference surface of like orientation. The light-loss fraction is the ratio of light loss to raw global solar irradiance. Put another way, the light-loss fraction is the product of the "direct fraction"—the ratio of raw direct solar irradiance to raw global solar irradiance—and the shade fraction. The ratio of daily light loss (energy per unit area) to raw daily global solar irradiation (energy per unit area) is the daily light-loss fraction; the ratio of annual light loss to raw annual global solar irradiation is the annual light-loss fraction.

Light loss in future years is estimated by repeating these calculations after simulating tree growth.

2.1 Spatial data selection

A well-treed residential neighborhood in each city containing a mix of single- and double-story tract homes built between 1980 and 1990 was selected. This provided study regions in which trees were about 20 years old when surface elevations were measured (2001 or 2005) and thus tall enough to shade the roofs of these typical modern homes. Google Earth aerial images of the study regions in Sacramento (2.7 km^2), San Jose (4.1 km^2), Los Angeles (3.7 km^2) and San Diego (3.1 km^2) are

shown in Figure 1.

2.2 Tree surveys

Urban tree surveys performed by city agencies, utilities, shade tree advocacy programs and urban foresters typically do not identify those trees that are both sufficiently close and tall enough to shade a roof. We conducted our own surveys by taking an expert arborist on a driving tour through about half of the streets in each study region. The arborist identified the species of each tree that we considered large enough and close enough to a house to possibly shade the roof. A limitation of this method is that we could clearly observe only the trees in the front or sides of the houses; we had no access to the backyards. However, most homes seemed to be on small lots with some lawn in front. This suggests that the back yards would tend to be too small for large trees.

Table 2 compiles the tree censuses performed in each of the four study regions. Also shown for each specie is the maximum height, growth rate and crown shape obtained from SelecTree tree selection guide [10] or from the Canopy tree library [11]. If there was a choice of subspecies, such as varieties of Ficus (fig) trees, we list the largest and fastest growing variety.

2.3 Spatial data acquisition

High-resolution digital color orthophotos and LiDAR (Light Detection And Ranging) measurements of surface elevation—i.e., height above sea level versus easting and northing—were collected by airplane-mounted instruments; parcel outlines were acquired from cities and counties (Table 1).

2.4 Shading analysis

The following analysis employed the ESRI ArcView 9.1 geographic information system (GIS) tool [12].

2.4.1 Roof, plane and tree outlines

The shapes (ground-plane projection outlines) of all roofs, planes and tree canopies were manually traced from high resolution color orthophotos rendered in the GIS tool. Figures 2 shows roof, plane, tree and parcel borders overlaid on a detail of the San Jose study region.

2.4.2 Elevation and height rasters

The year of the LiDAR survey—2001 in Sacramento, 2005 elsewhere—is denoted year zero. A year-zero raster of surface elevation (surface height above sea level) spanning the study region was computed via inverse-distance-weighted interpolation of the LiDAR surface elevation measurements (Figure 3). All generated rasters contain square cells 50 cm on a side.

A ground-elevation raster (ground height above sea level) was computed as the 50-m focal minimum of the surface-elevation raster and the surface-height raster (surface height above ground) was computed by subtracting the ground-elevation raster from the surface-elevation raster. The study-region surface-elevation raster was then disaggregated by parcel to create a set of several thousand "parcel" surface-elevation rasters.

Additional rasters of surface elevation were constructed to account for tree growth after 10, 20 and 30 years. Tree height h at age t was approximated with the asymptotic growth model

$$h(t) = H\left[1 - \exp\left(-t/\tau\right)\right] \tag{1}$$

where H is the mature height of the tree. In this model, the time constant τ, or age at which the tree reaches about 63% of its mature height, is equal to the ratio of the tree's mature height H to its initial growth rate. Tree-canopy width was not increased over time in our analysis.

If the height of the tree at age t_0 is known to be h_0, the time constant τ can be eliminated from Eq. (1) to yield

$$h(t) = H\left[1 - \left(1 - h_0/H\right)^{t/t_0}\right]. \tag{2}$$

Assuming that all trees were planted when the homes were built made them about 20 years old in year zero. Each tree's height at this age was estimated as the maximum year-zero surface height-above-ground of cells within its traced border.

An upper limit to future-year shading was estimated with Eq. (2) by applying to all trees the mature height associated with the tallest species of trees found in the study regions (H = 20 m). The relationship between future height $h(t)$ and initial height h_0 for trees with mature height H = 20 m and initial age t_0 = 20 years is shown in Figure 5. With these assumptions, any tree that is at least 10 m tall in year 0 will approach its mature height of 20 m by year 30. Since the mean LiDAR-derived treetop height in year 0 was 10±4 m in Sacramento, 12±6 m in San Jose, 15±6 m

in Los Angeles and 14±5 m in San Diego, the model predicts more tree growth in the Sacramento and San Jose than in Los Angeles and San Diego.

Future-year rasters of surface height above ground were generated by "growing" the trees in the year-zero raster of surface height above ground. Future-year surface elevation (above sea level) was then calculated by adding future-year surface height above ground to year-zero ground elevation.

2.4.3 Plane aspect

A vector was drawn to the centroid of each plane shape from the centroid of the roof shape containing that plane. The azimuthal angle of that vector was binned into a 45-wide aspect—N, NE, E, SE, S, SW, W or NW—indicating the side of the roof on which the plane lies. This method was found to be more reliable than determining aspect by fitting a planar surface through the subset of LiDAR points that lie above the plane's shape.

Table 3 shows the distribution of planes by aspect in each study region.

2.4.4 Shadow rasters

The National Renewable Energy Laboratory's Solar Position and Intensity (SOLPOS) calculator [13] was used to compute on-hour solar positions at the center of the study area to within 0.01°. The Hillshade function of the GIS tool was then used to determine from solar position whether any cell in a surface elevation raster lay in shadow. For each daylight hour in the 21st day of each month (143 hours/year), a raster of "total" shading—value 1 if the cell lies in the shadow of any cell in the study region; 0 otherwise—was computed from the study-region surface-elevation raster. Figure 6 illustrates on-hour total shading in San Jose at 9A, 12P, 3P and 5P local standard time (LST) on June 21.

A second raster of "intraparcel" shading—value 1 if the cell lies in the shadow of another cell within its own parcel; 0 otherwise—was generated by aggregating shadow rasters computed from the individual parcel surface-elevation rasters. Intraparcel shadow rasters were computed for only 15 hours/year—the daylight subsets of 9A, 12N, 3P and 6P LST on the 21st days of March, June, September and December—because the time required to calculate intraparcel shading was about three orders of magnitude longer than that required to compute total shading. Figure 7 shows intraparcel shading in San Jose at 5P LST on June 21.

On-hour "extraparcel" shadow rasters were computed by subtracting the on-hour intraparcel shadow rasters from the on-hour total shadow rasters (Figure 8). Scattered values of -1 (red cells) and 1 (black cells) in the extraparcel shadow raster are artifacts of the shadow modeling process that result from small registration errors.

2.4.5 Shade fraction and light loss of each plane

The on-hour total, intraparcel and extraparcel shade fractions of each roofing plane were computed by averaging the values of the plane's cells in the corresponding shadow raster. On-hour values of global-tilt solar irradiance (incident solar power/area) incident on unshaded, 5:12 pitch roofing planes in each of the eight aspects were computed with the Hay-Davies-Klutcher-Reindl radiation model [14] embedded in the California Energy Commission's CECPV 2.3 solar calculator [15]. On-hour values of the direct-tilt solar irradiance incidence on these surfaces were computed from consideration of solar position, plane orientation and the direct-normal solar irradiances values contained in the weather files bundled with the CECPV calculator. To reduce artifacts that can result from cloudy weather on a particular day, each on-hour irradiance was smoothed by calculating an hour-of-day running average over an interval of -15 days to +15 days.

Total, intraparcel and extraparcel instantaneous light losses (loss of incident solar power/area) were calculated by multiplying each on-hour shade fraction by the aspect-appropriate smoothed on-hour direct-tilt solar irradiance. Corresponding instantaneous light-loss fractions were computed by dividing each light loss by the aspect-appropriate smoothed on-hour raw global-tilt solar irradiance.

2.4.6 Light loss and light-loss fraction of a set of planes

The on-hour mean light-loss fraction of a set of roofing planes, or fraction by which shading reduces the aggregate solar power incident on the planes at that hour, is the ratio of the planes' aggregate light loss—set sum of the product of each plane's on-hour shade fraction, on-hour raw direct-tilt solar irradiance and surface area—to the planes' aggregate raw global-tilt solar irradiance (set sum of the product of each plane's on-hour raw global-tilt solar irradiance and surface area). On-hour mean total, intraparcel and extraparcel light-loss fractions were computed for the subsets of roofing planes in each of the eight aspects.

The mean light-loss fraction F of a set of roofing planes over some time interval, or fraction by

which shading reduces the aggregate solar energy incident on these planes, is the ratio of the time integral of the planes' aggregate light loss to the time integral of the planes' aggregate raw global-tilt solar irradiance. Daily mean total light-loss fractions for the subsets of roofing planes in each of the eight aspects were evaluated the 21st day of each month. Intraparcel and extraparcel values were evaluated on the 21st days of March, June, September and December. Annual mean light-loss fractions were evaluated by integrating over all hours of the year for which on-hour light-loss fractions were computed.

2.4.7 Solar access violation

California Public Resources Code §25982 [16] states that, subject to certain exceptions,

> . . .no person owning, or in control of a property shall allow a tree or shrub to be placed, or, if placed, to grow on such property, subsequent to the installation of a solar collector on the property of another so as to cast a shadow greater than 10 percent of the collector absorption area upon that solar collector surface on the property of another at any one time between the hours of 10 a.m. and 2 p.m., local standard time. . .

The solar access of a roofing plane was considered violated in a given month if its extraparcel shade fraction exceeded 10% at any time between 10A and 2P LST on the 21st day of that month. Since extraparcel shading was calculated only at 9A, 12N, 3P and—except in December—6P LST, extraparcel shade fractions at 10A, 11A, 1P and 2P LST were interpolated from the calculated values.

3 Results

3.1 Special characteristics of S-, SW- and W-facing planes

The following analysis pays special attention to the "S+SW+W" subset of roofing planes that face S, SW or W, because solar equipment is commonly installed on such planes for maximum solar access. For example, assuming a plane slope of 5:12, annual mean raw global solar irradiance in the four study regions is greatest for S-facing planes; values for SW-, SE-, W- and E-facing planes are 3 - 5%, 5 - 7%, 10 - 15% and 15 - 20% lower, respectively (Figure 9). However, the raw global solar irradiances received by SW- and W-facing planes can exceed that incident on a S-facing planes

during times of peak electrical demand, such as late afternoon in summer. We note also that daily mean global solar irradiance on S+SW+W-facing planes on December 21 (the winter solstice) is only about 30% of that on June 21 (the summer solstice).

The S-, SW- and W-facing planes in the four regions generally have higher direct fractions—that is, receive greater proportions of their global solar irradiances in the form of direct sunlight—than do planes of other orientations (Figure 10). Since light-loss fraction is the product of shade fraction and direct fraction, these high values of direct fraction can in some circumstances make the light-loss fraction of a S-, SW- or W-facing plane exceed that of, say, a N-facing plane.

3.2 On-hour light-loss fractions and light losses of S+SW+W-facing planes in years 0 and 30

Since direct fraction increases and shadow length decreases with solar altitude, on-hour total light-loss fraction (shade fraction times direct fraction) was typically lowest near sunrise and sunset, when direct fraction is small and around noon, when shadows are shortest. On-hour total light-loss fractions typically peaked about one to two hours after sunrise and one to two hours before sunset (Figure 11). In year 0, the maximum values of on-hour total light-loss fraction were 0.43 in Sacramento, 0.44 in San Jose, 0.25 in Los Angeles and 0.55 in San Diego. In year 30, they reached 0.46 in Sacramento, 0.47 in San Jose, 0.34 in Los Angeles and 0.58 in San Diego. Between year 0 and year 30, individual on-hour total light-loss fractions increased by up to 0.15 in Sacramento, 0.13 in San Jose, 0.09 in Los Angeles and 0.14 in San Diego.

On-hour total light loss (shade fraction times direct solar irradiance) vanished at sunrise and sunset, when there was no direct sunlight. On the spring, summer and autumn days, on-hour total light loss typically peaked about two to four hours after sunrise and about two to four hours before sunset, with a midday trough near noon. On the winter day, the shapes of the on-hour total light loss curves were complicated by the influence of cloudy weather on direct solar irradiance (Figure 11). In year 0, the maximum values of on-hour total light loss were 71 W m^{-2} in Sacramento, 65 W m^{-2} in San Jose, 85 W m^{-2} in Los Angeles and 72 W m^{-2} in San Diego. In year 30, they reached 140 W m^{-2} in Sacramento, 109 W m^{-2} in San Jose, 125 W m^{-2} in Los Angeles and 115 W m^{-2} in San Diego. Between year 0 and year 30, individual on-hour total light losses increased by up to 78 W m^{-2} in Sacramento, 45 W m^{-2} in San Jose, 46 W m^{-2} in Los Angeles and 48 W m^{-2} in San

Diego.

On-hour extraparcel light-loss fractions were very small in year 0; all values were less than 0.05 except for two peaks of about 0.13. In year 30, all values were less than 0.10, except for two peaks of 0.15. Between year 0 and year 30, individual extraparcel light-loss fractions increased by up to 0.05 in Sacramento, 0.04 in San Jose, 0.03 in Los Angeles and 0.04 in San Diego. On-hour extraparcel light losses were also very small, never exceeding 10 W m^{-2} in year 0 and 25 W m^{-2} in year 30. Between year 0 and year 30, individual extraparcel light losses increased by up to 15 W m^{-2} in Sacramento, 11 W m^{-2} in San Jose, 8 W m^{-2} in Los Angeles and 16 W m^{-2} in San Diego.

3.3 Daily light-loss fractions for S+SW+W-facing planes in years 0, 10, 20 and 30

Figure 12 plots for each study region the daily total and extraparcel light-loss fractions for the S+SW+W subset of planes on the 21st day of each month in years 0, 10, 20 and 30.

Daily light-loss fractions are greatest in winter and least in summer because at a given hour of the day, the sun is lower and shade fractions are greater—that is, shadows are longer—in winter than in summer. However, since light-loss fraction is the product of shade fraction and direct fraction, seasonal variations in direct fraction (Figure 10) can augment or decrease daily light-loss fractions. For example, the S+SW+W set of planes in Sacramento receives 78% of its global solar irradiance as direct sunlight on June 21, but only 63% on December 21, diminishing the winter-summer difference in light-loss fraction. San Jose has a similar pattern, with direct fractions of 78% on June 21 and 60% on December 21. Variations in direct fraction tend to increase the winter-summer differences in light-loss fraction in Los Angeles and San Diego, where direct fractions are lower in summer than in winter (64% vs. 72% in Los Angeles, 65% vs. 79% in San Diego). These effects make the Los Angeles and San Diego light-loss fraction curves in Figure 12 more elliptical than those for Sacramento and San Jose.

Over the course of the year, daily total light-loss fractions of S+SW+W planes in year 0 were 0.05 - 0.14 in Sacramento, 0.05 - 0.15 in San Jose, 0.05 - 0.15 in Los Angeles and 0.04 - 0.16 in San Diego; the range over all regions was 0.04 - 0.16. By year 30, values increased to 0.09 - 0.26 in Sacramento, 0.08 - 0.23 in San Jose, 0.07 - 0.23 in Los Angeles and 0.05 - 0.25 in San Diego; the range over all regions was 0.06 - 0.25.

Daily extraparcel light-loss fractions of S+SW+W planes in year 0 were 0.00 - 0.03 in Sacramento, 0.01 - 0.02 in San Jose, 0.00 - 0.01 in Los Angeles and 0.00 - 0.01 in San Diego; the range over all regions was 0.00 - 0.03. By year 30, values increased to 0.01 - 0.06 in Sacramento, 0.01 - 0.05 in San Jose, 0.01 - 0.03 in Los Angeles and 0.01 - 0.04 in San Diego; the range over all regions was 0.01 - 0.06.

3.4 Daily light-loss fractions by aspect in years 0 and 30

Figures 13 and 14 plot for each study region the daily total and extraparcel light-loss fractions by aspect on March 21, June 21, September 21 and December 21 in years 0 and 30, respectively.

The shape of each curve of daily light-loss fraction versus aspect depends on the hourly solar trajectory, the hourly direct fraction and surface topography—that is, the relative heights and locations of buildings and trees. The solar trajectory in Sacramento (latitude 38.5°N) is similar to that in San Jose (latitude 37.3°N) and the solar trajectory in Los Angeles (latitude 34.0°N) is similar to that in San Diego (latitude 33.0°N). There is some similarity between the hourly direct fractions in Sacramento and San Jose and little between the hourly direct fractions for any other pair of cities (Figure 10). There is no reason to expect the surface topographies in any two cities to be alike. Hence, it is unsurprising that the curves of daily light-loss fraction versus aspect differ strongly from city to city in Figures 13 and 14.

Daily light-loss fractions in every aspect were generally smallest in summer and largest in winter, with intermediate values in spring and autumn. Two prominent features in these curves—the autumn-spring differences in daily light loss fractions and the dips in light-loss fraction on December 21 for N-facing planes—can be traced to the charts of direct fraction versus aspect shown in Figure 10.

Over the four study regions, year 0 daily total light-loss fractions by aspect were 0.03 - 0.08 on June 21, 0.06 - 0.14 on March 21, 0.05 - 0.12 on September 21 and 0.06 - 0.20 on December 21. In year 30, these values increased to 0.05 - 0.11 on June 21, 0.10 - 0.17 on March 21, 0.08 - 0.16 on September 21 and 0.07 - 0.26 on December 21. Year 0 daily extraparcel light-loss fractions were 0.00 - 0.01 on June 21, 0.00 - 0.02 on March 21, 0.00 - 0.01 on September 21 and 0.00 - 0.03 on December 21. In year 30, these values increased to 0.00 - 0.02 on June 21, 0.00 - 0.03 on March 21, 0.00 - 0.02 on September 21 and 0.00 - 0.06 on December 21.

For the subset of S+SW+W-facing planes in the four study regions, year 0 daily total light-loss fractions were 0.04 - 0.06 on June 21, 0.07 - 0.10 on March 21, 0.06 - 0.08 on September 21 and 0.14 - 0.16 on December 21. In year 30, these values increased to 0.05 - 0.09 on June 21, 0.11 - 0.14 on March 21, 0.09 - 0.15 on September 21 and 0.23 - 0.26 on December 21. Year 0 daily extraparcel light-loss fractions were 0.00 - 0.01 on June 21, March 31 and September 21 and 0.01 - 0.03 on December 21. In year 30, these values increased to 0.00 - 0.01 on June 21, 0.01 - 0.02 on March 21 and September 21 and 0.03 - 0.06 on December 21.

3.5 Annual light-loss fractions by aspect in years 0, 10, 20 and 30

Figure 15 plots for each study region the annual total and extraparcel light-loss fractions by aspect in years 0, 10, 20 and 30. Differences in hourly solar trajectory, hourly direct fraction and surface topography all tend to make curves of annual light-loss fraction in each year vary from region to region. However, the most prominent feature in this figure—that light-loss fractions increased more from year 0 to year 30 in Sacramento and San Jose than in Los Angeles and San Diego—resulted from greater tree growth in the first two cities (c.f. §2.4.2).

Over the four study regions, annual total light-loss fractions by aspect were 0.06 - 0.10 in year 0, 0.08 - 0.12 in year 10, 0.09 - 0.13 in year 20 and 0.09 - 0.14 in year 30. Annual extraparcel light-loss fractions were 0.00 - 0.01 in year 0 and 0.00 - 0.02 in years 10, 20 and 30.

For the subset of S+SW+W-facing planes in the four study regions, annual total light-loss fractions were 0.07 - 0.08 in year 0, 0.09 - 0.10 in year 10, 0.10 - 0.12 in year 20 and 0.11 - 0.14 in year 30. Annual extraparcel light-loss fractions were 0.01 in years 0 and 10 and 0.01 - 0.02 in years 20 and 30.

3.6 Daily solar access violations by aspect

Figures 16 and 17 plot for each study region the rates of solar access violation by aspect on March 21, June 21, September 21 and December 21 in years 0 and 30, respectively.

Rates of solar access violation were much higher on December 21 than on the three other days because the sun is low and mid-day shadows are long in winter. Over the four study regions, year 0 rates of solar access violation by aspect were 0 - 3% on June 21, 1 - 7% on March 21, 1 - 6% on September 21 and 4 - 31% on December 21. By year 30, these values increased to 0 - 4% on June

21, 2 - 19% on March 21, 3 - 20% on September 21 and 12 - 56% on December 21.

For S+SW+W-facing planes, year 0 rates of solar access violation were 1% on June 21, 2 - 5% on March 21, 3 - 5% on September 21 and 11 - 28% on December 21. By year 30, these values increased to 1 - 3% on June 21, 6 - 16% on March 21, 7 - 16% on September 21 and 29 - 55% on December 21.

4 Conclusions

Tree growth increased annual total light-loss fractions for the S+SW+W-facing planes by about 50 to 70% over 30 years, from 0.07 - 0.08 in year 0 to 0.11 - 0.14 in year 30. Annual extraparcel light-loss fractions very slightly increased from 0.01 in years 0 to 0.01 - 0.02 in year 30. Trees and buildings in neighboring parcels are responsible for only about 10% of the annual light loss of these roofing planes (i.e., annual extraparcel shade fraction / annual total shade fraction $\approx$ 10%).

Shading degrades solar access least in summer, which abets the production of electricity to meet peak demand in the cooling season. For example, daily total light-loss fractions for S+SW+W-facing planes in year 0 were 0.04 - 0.06 on June 21 and 0.14 - 0.16 on December 21, increasing by year 30 to 0.05 - 0.09 on June 21 and 0.23 - 0.26 on December 21.

Long winter shadows yield high rates of solar access violation on December 21. For example, year 0 rates of solar access violation for S+SW+W-facing planes were 1% on June 21 and 11 - 28% on December 21, increasing by year 30 to 1 - 3% on June 21 and 29 - 55% on December 21. High rates of violation in winter do not greatly reduce annual solar access because the daily mean global solar irradiance on December 21 is less than a third of that on June 21.

In spring, summer and autumn, total light loss for S+SW+W-facing planes peaks about two to four hours after sunrise and about two to four hours before sunset. In summer, the light loss fraction in late afternoon (when demand for cooling electricity is particularly high) is about twice the fraction of light lost over the entire day. For example, on June 21 of year 0 in San Jose, the light loss fraction at 5P LST is 0.12, while that for the entire day is 0.06. This suggests that daily or annual light loss fractions may not properly capture the influences of shading on solar access during peak demand hours. Future work could gauge the economic losses that result from shading by weighting hourly light loss with the time-dependent value of electricity.

5 Acknowledgements

This work was supported by the California Energy Commission (CEC) through its Public Interest Energy Research Program (PIER) and by the Assistant Secretary for Energy Efficiency and Renewable Energy under Contract No. DE-AC02-05CH11231. We thank Bill Pennington of the California Energy Commission for helping to organize the study and for his guidance and support. For identifying trees, we thank Dan Pskowski, arborist, City of Sacramento; Ralph Mize, arborist, City of San Jose; David Lofgren, arborist, Los Angeles County Arboretum; and Drew Potocki, arborist, City of San Diego. For providing spatial data, we thank Nathan Jennings, City of Sacramento; Kevin Briggs and Roland Gong, City of San Jose; and Lisa Lubeley, City of San Diego. Finally, we thank Kimberly Fujita for tracing the outlines of roughly 100,000 roofs, planes and trees in our study-region images.

References

[1] R.J. Kaye, R. O'Brien, N. Ghiotto, and P. McKee. Site selection and assessment of rooftop photovoltaic installations. In *Proceedings of the 14th European Photovoltaic Solar Energy Conference and Exhibition*, Barcelona, Spain, 30 June - 4 July 1997.

[2] J. Mardaljevic and M. Rylatt. Irradiation mapping of complex urban environments: an image-based approach. *Energy & Buildings*, 35:27–35, 2003.

[3] R. Compagnon. Solar and daylight availability in the urban fabric. *Energy & Buildings*, 36:321–328, 2004.

[4] CH2MHill. CH2MHill Solar Automated Feature Extraction ^{TM} technology. `http://www.ch2m.com`, 2008.

[5] J.R. Simpson. Improved estimates of tree-shade effects on residential energy use. *Energy & Buildings*, 34:1067–1076, 2002.

[6] H. Akbari. Shade trees reduce building energy use and CO_2 emissions from power plants. *Environmental Pollution*, 116:S119–S126, 2002.

[7] E.G. McPherson and J.R Simpson. Potential energy savings in buildings by an urban tree planting programme in California. *Urban Forestry & Urban Greening*, 2:73–86, 2003.

[8] H. Akbari, L.S. Rose, and H. Taha. Analyzing the land cover of an urban environment using high-resolution orthophotos. *Landscape & Urban Planning*, 63:1–14, 2003.

[9] L.S. Rose, H. Akbari, and H. Taha. Characterizing the fabric of the urban environment: a case study of greater Houston, Texas. Report LBNL-51448, Lawrence Berkeley National Laboratory, Berkeley, CA, 2003.

[10] UFEI. Selectree: a tree selection guide. `http://selectree.calpoly.edu`, 2008. Urban Forests Ecosystem Institute, California Polytechnic State University, San Luis Obispo, CA.

[11] Canopy. Canopy tree library. `http://www.canopy.org`, 2008. Palo Alto, CA.

[12] ESRI. ESRI ArcView 9.1 geographic information system. `http://www.esri.com`, 2008.

[13] NREL MIDC. National Renewable Energy Laboratory Measurement and Instrumentation Data Center (NREL MIDC) Solar Position and Intensity (SOLPOS) Calculator. Online at `http://www.nrel.gov/midc/solpos/solpos.html`, 2008.

[14] J.A. Duffie and W.A. Beckman. *Solar Engineering of Thermal Processes*. John Wiley & Sons, 3rd edition, 2006.

[15] B.A. Wilcox and W.A. Beckman. California Energy Commission CECPV Calculator 2.3. `http://www.gosolarcalifornia.ca.gov/nshpcalculator/download_calculator.html`, 2008.

[16] CPRC. California Public Resources Code §25982. `http://www.leginfo.ca.gov/cgi-bin/displaycode?section=prc&group=25001-26000&file=25980-25986`, 2008.

	Sacramento	San Jose	Los Angeles	San Diego
area (km^2)	2.7	4.1	3.7	3.1
center	38.50°N, 121.54°W	37.31°N, 121.78°W	34.03°N, 117.88°W	32.96°N, 117.14°W
parcel count	2,461	3,705	2,169	2,554
roof count	2,411	3,610	2,120	2,538
plane count	10,626	17,998	8,619	10,151
tree count	7,263	11,200	11,588	9,304
parcel shape date	March 2005	January 2006	March 2006	January 2006
parcel shape source	City of Sacramento	City of San Jose	Los Angeles County	SanGIS (city and county of San Diego)
orthophoto flight date	March 2001	March 2001	November 2005	March - May 2005
orthophoto source	Horizons, Inc. via City of Sacramento	Triathlon Ltd. via City of San Jose	Optimal Geomatics	Merrick and Company via City of San Diego
orthophoto pixel size (cm) [in]	15.2 × 15.2 [6 × 6]	7.6 × 7.6 [3 × 3]	7.6 × 7.6 [3 × 3]	7.6 × 7.6 [3 × 3]
LiDAR flight date	March 2001	October 2005	November 2005	March - May 2005
LiDAR source	Horizons, Inc. via City of Sacramento	Airborne1	Optimal Geomatics	Merrick and Company via City of San Diego
LiDAR horizontal spacing (m)	4	1.4	0.87	1.5
LiDAR horizontal accuracy (m)	0.4	0.46	0.6	1.2
LiDAR vertical accuracy (m)	0.2	0.36	0.12	0.36
LiDAR points in study region	338,279	8,308,823	10,143,843	4,797,743
LiDAR density (points/m^2)	0.1	2.0	2.7	1.6
notes	Pocket Road area		City of Walnut	

Table 1: Characteristics of study regions in four California cities.

	Maximum height (m)	Growth rate (cm/season)	Crown shape	Sacramento	San Jose	Los Angeles	San Diego
Alder White	20	94	conical	3		4	1
Ash, Evergreen	20	94	oval		1		11
Ash, Raywood	11	61	oval	2	3	1	
Ash, Shamel	20	91	oval	1	3		
Birch, N. European	15	91	oval			1	
Birch - White	15	91	oval	17	2		
Bottlebrush	8	91	oval			1	
Box, Brisbane	15	91	oval				8
Camphor	20	61	rounded	2	1		
Carrot Wood	11	61	oval			9	2
Cedar, Blue Atlas	20	61	conical		1		
Cedar, Deodar	>20	91	conical		3		
Cherry, Flowering	8	91	umbrella	1			
Chinese Flame	11	61	rounded				1
Chinese Hackberry	20	61	rounded	4			
Chinese Pistache	20	61	oval		1		
Chinese Tallow	11	61-91	conical	5			
Crape Myrtle	8	61	oval	1	1		
Cypress, Italian	15	91	columnar		9	18	1
Cypress, Leyland	>20	91	conical				6
Elm, Chinese	20	>94	oval		3		
Ericaceae (Madrone)	20	61	round			6	
Eucalyptus,	>20	>94	oval		6	15	5
Ficus (Fig)	20	>94	rounded			8	1
Ginko	20	91	columnar			1	
Honey Locust	20	91	oval	3			
Jacaranda	15	61	oval		1	6	1
Juniper, California	11	61	conical			2	
Liquidambar	20	91	conical	8		3	
London Plane	20	91	oval	4	1		
Magnolia	20	61	oval	1	1	1	
Maple, Silver	20	>94	oval		4		
Oak, Coast Live	20	61	rounded		1		
Oak, Red	20	61-91	oval	1			
Oak, Silk	20	91	oval	1			
Oak, Valley	>20	91	oval		2		
Oak, Holly	20	61	rounded	1	1		
Palm, King	20	61	feather palm			10	1
Palm, Mexican	>20	>94	fan palm				3
Palm, Queen	15	91	feather palm				2
Pear Ornamental (Aristocrat)	15	61-91	conical	2	1		
Pepper, Californian	15	91	rounded		2	2	
Pine, Canary Island	20	91	columnar		3	1	15
Pine, Italian Stone	>20	91	conical		1	10	2
Pine, Japanese Black	15-20	61-91	conical	2			
Pine, Monterey	>20	>94	conical		4	8	
Pine, Norfolk Island	>20	61	conical				1
Pine, Torrey	20	91	conical				3
Pittosporum	11	61	oval			1	
Plum Purple Leaf	11	61-91	oval	1			
Podocarpus, Latifolius	20	61	conical			4	
Privet, Glossy	15	91	oval		1		
Redwood, Coast	>20	91	conical	7	12		
Sequoia	>20	91	conical			1	
Sycamore, Ca, Yarwood	>20	91	oval		2	6	
Tulip	20	91	conical	1			
Walnut, CA Black	20	61	rounded		1		
Willow, Australian	11	91	oval		1	1	
Total				**68**	**73**	**120**	**64**

Table 2: Growth characteristics and counts of tree species cataloged in ground surveys.

	Sacramento	San Jose	Los Angeles	San Diego
S+SW+W	36.4	38.5	37.8	37.7
S	14.7	15.8	14.5	14.3
SW	11.6	12.1	12.4	12.0
W	10.2	10.7	11.0	11.4
NW	12.7	12.1	11.8	12.0
N	15.1	14.3	13.8	14.0
NE	12.3	11.7	12.3	11.7
E	11.5	10.6	11.6	12.3
SE	11.9	12.8	12.7	12.3

Table 3: Fraction (%) of planes by aspect in each study region.

Figure 1: Aerial views of study regions in (a) Sacramento, (b) San Jose, (c) Los Angeles and (d) San Diego.

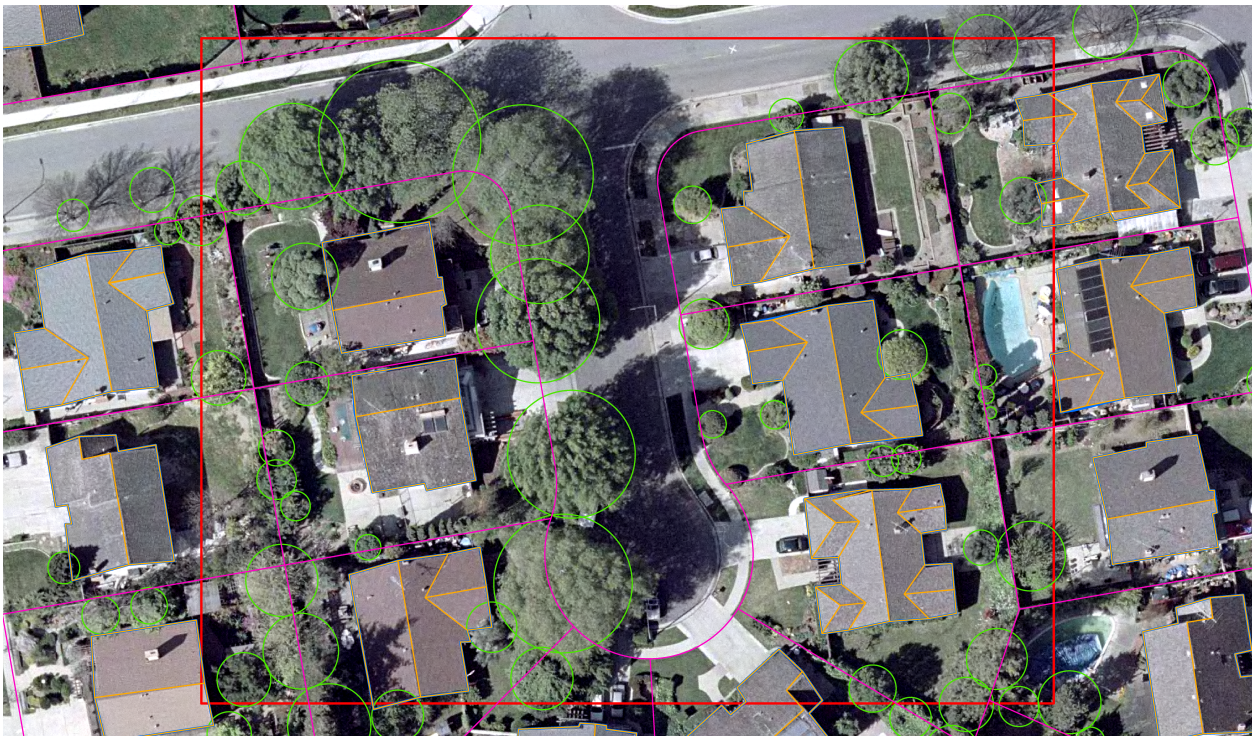

Figure 2: Roof (blue), plane (gold), tree (green) and parcel (magenta) shapes overlaid on detail of San Jose orthophoto.

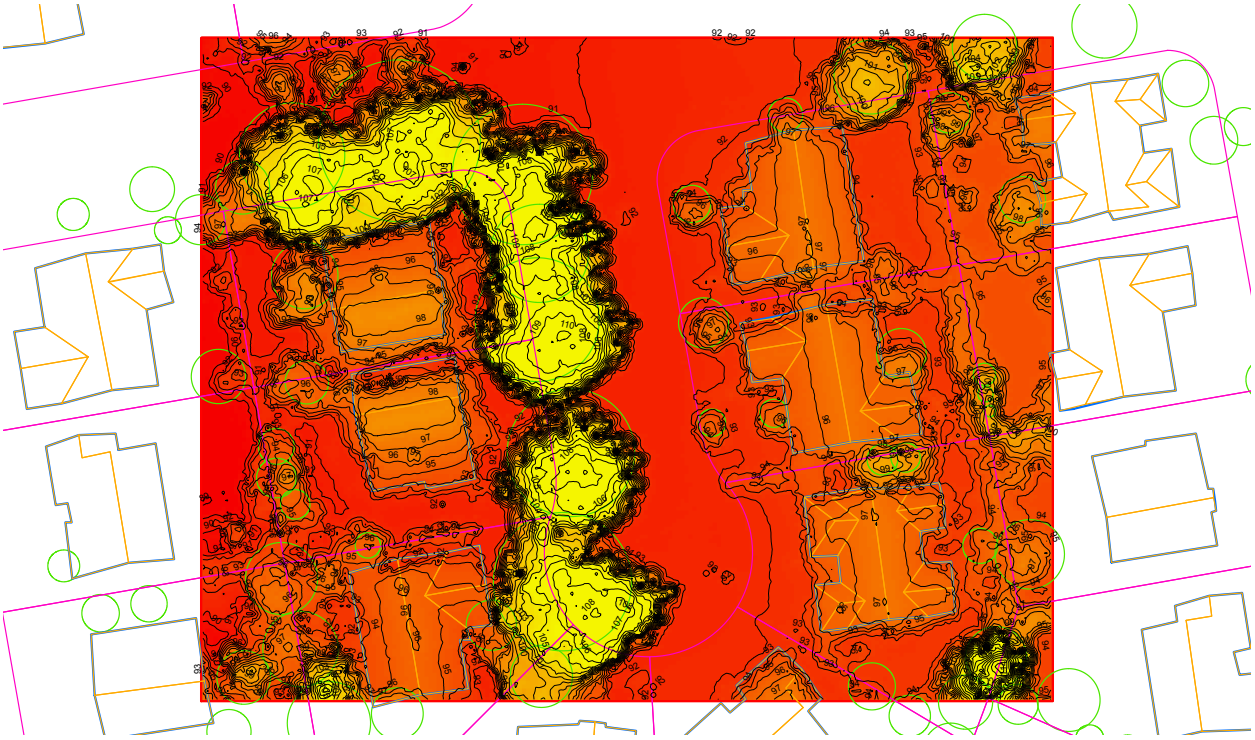

Figure 3: Detail of San Jose surface elevation raster (meters above sea level).

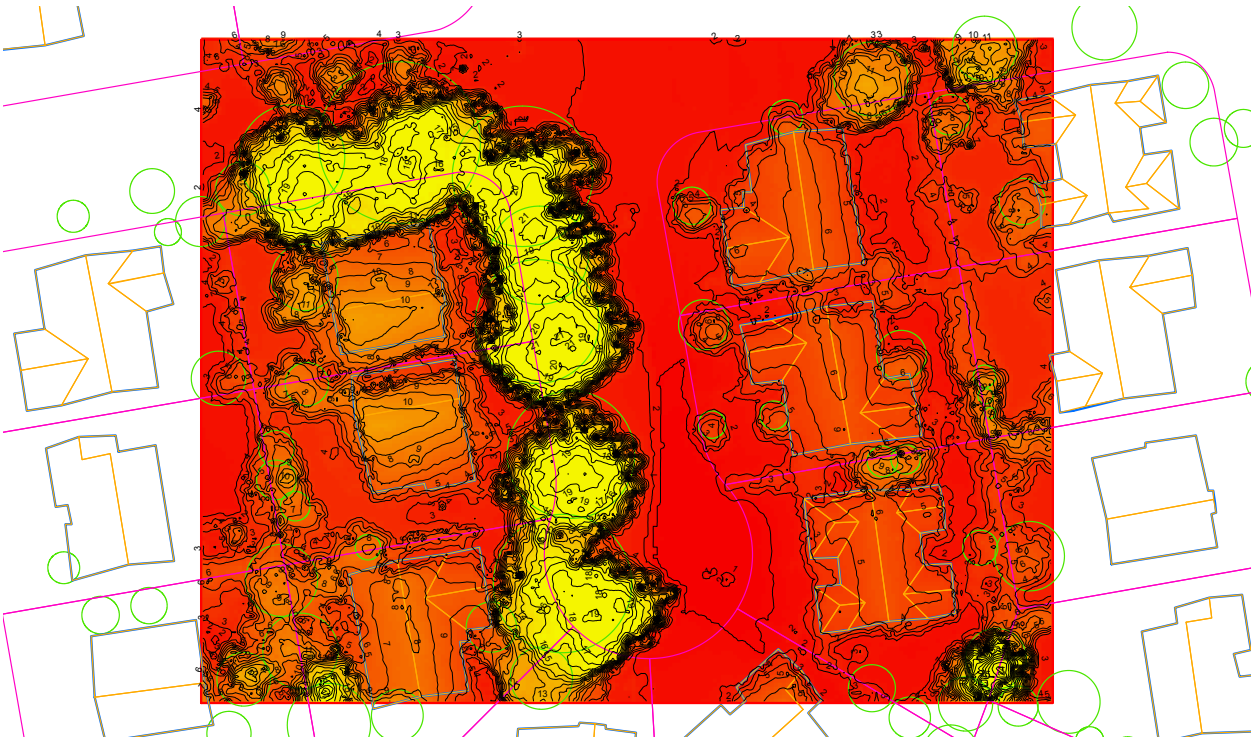

Figure 4: Detail of San Jose surface height raster (meters above ground).

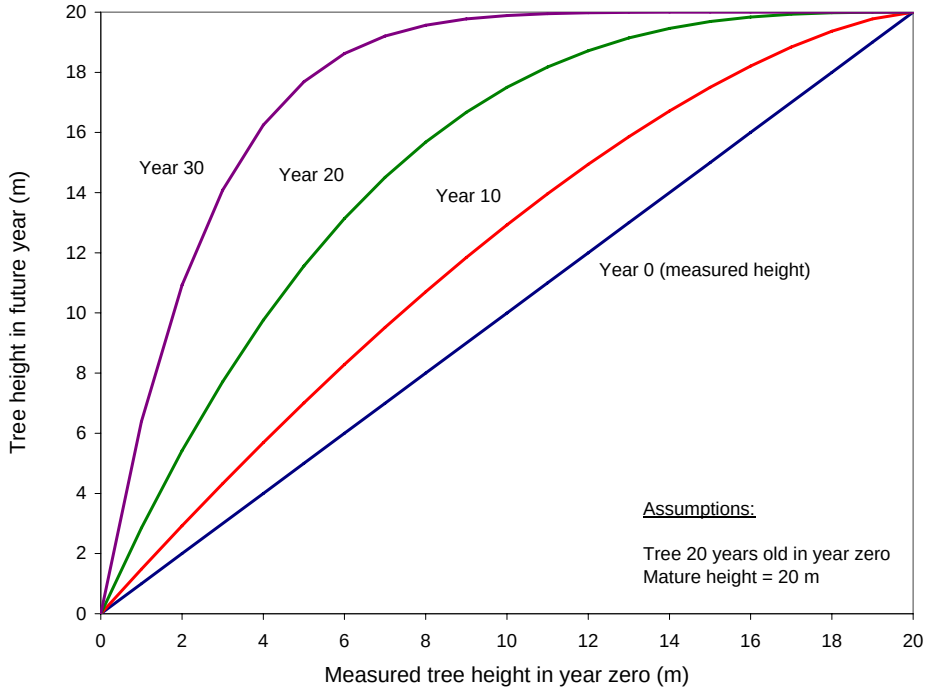

Figure 5: Asymptotic growth of tree that is 20 years old in year zero, assuming a mature height of 20 m.

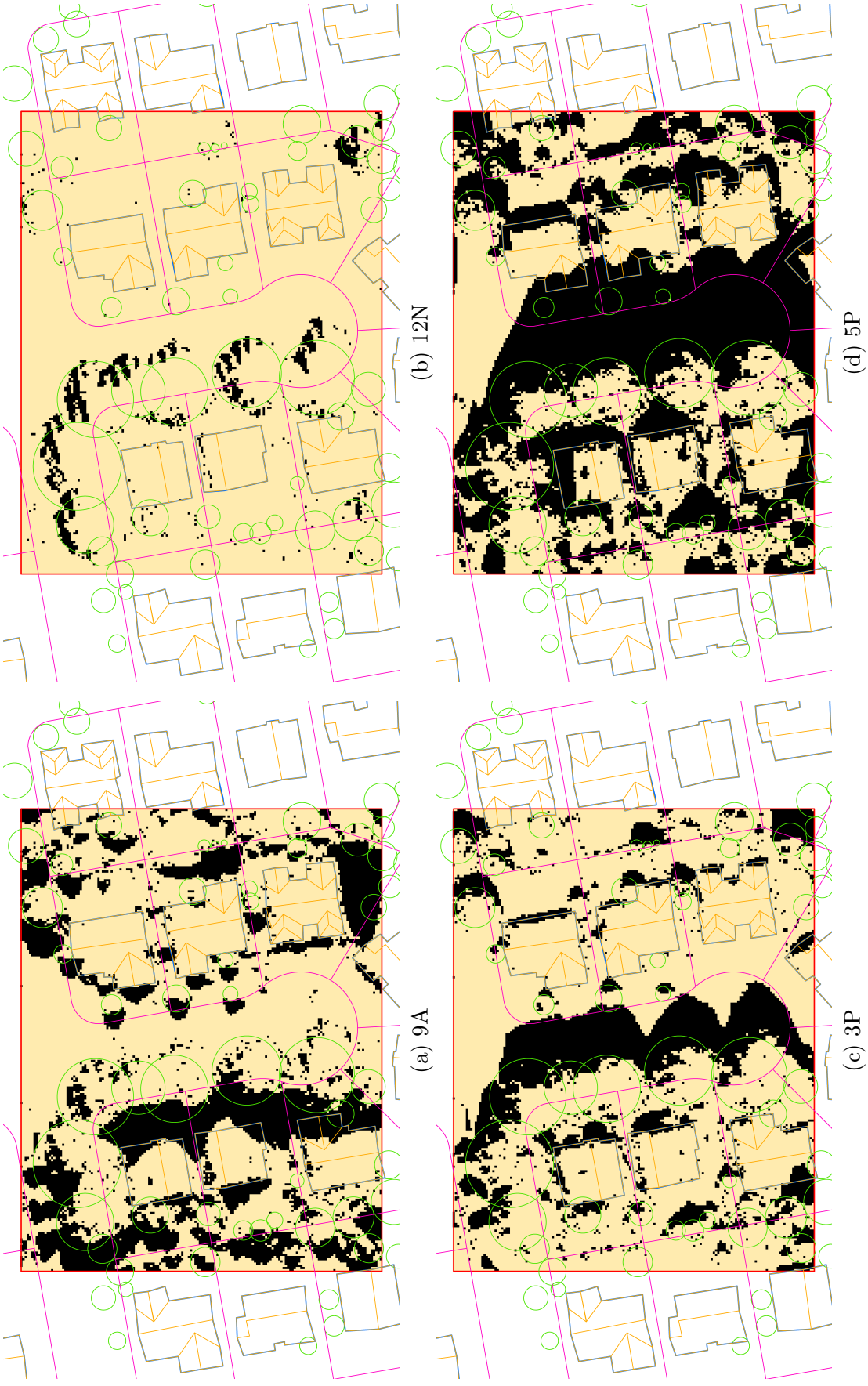

Figure 6: Details of San Jose total shadow rasters on June 21 at (a) 9A, (b) 12N, (c) 3P and (d) 5P local standard time. Black cells are shaded.

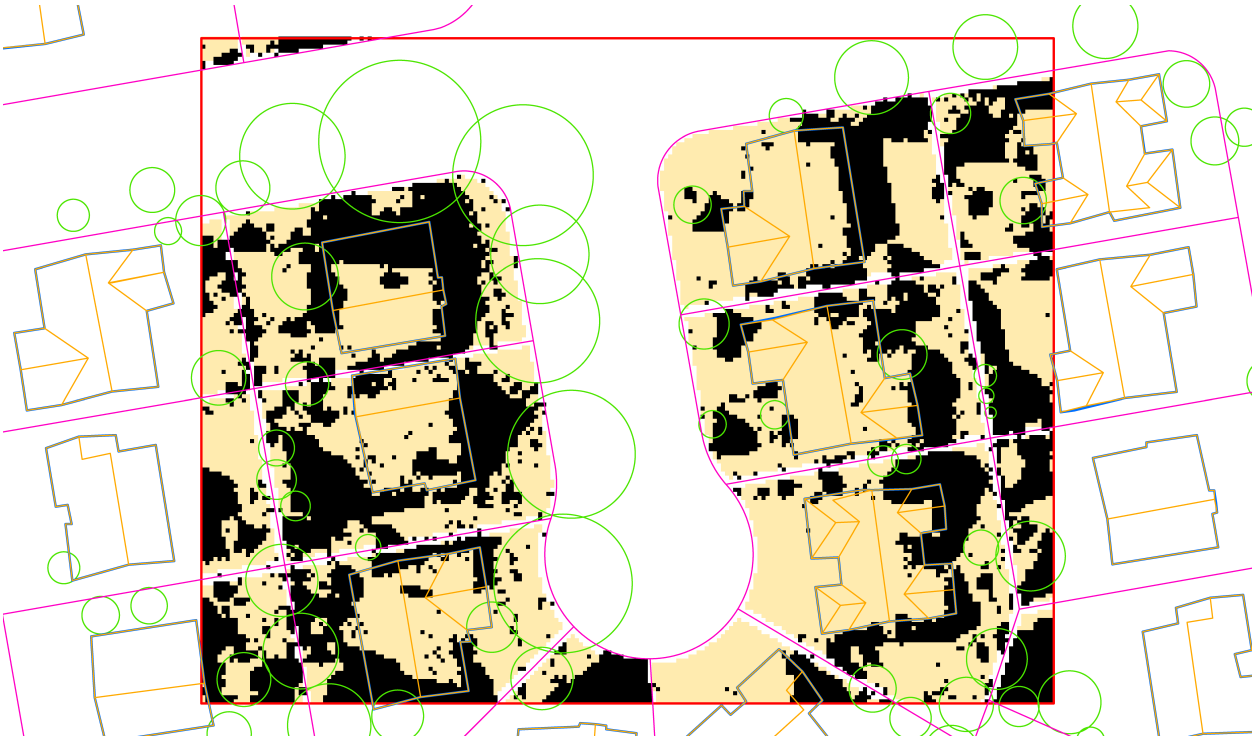

Figure 7: Detail of San Jose intraparcel shadow raster on June 21 at 5P LST. Black cells are shaded.

Figure 8: Detail of San Jose extraparcel shadow raster (total shadow raster minus intraparcel shadow raster) on June 21 at 5P LST. Black cells are shaded; isolated black cells and all red cells are computational artifacts.

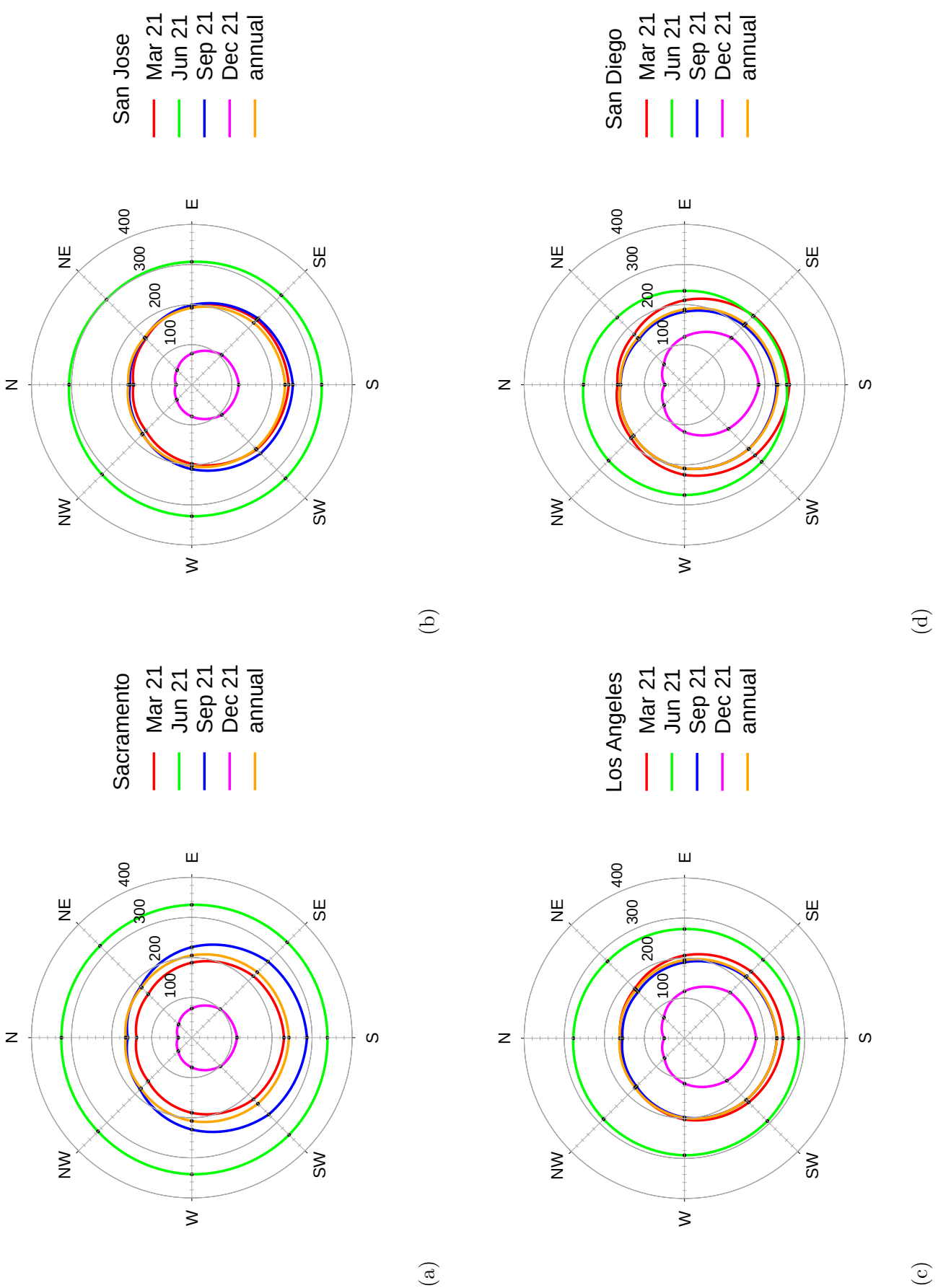

Figure 9: Daily and annual mean global solar irradiances (W m^{-2}) by aspect on unshaded 5:12 pitch roofing planes in (a) Sacramento, (b) San Jose, (c) Los Angeles and (d) San Diego.

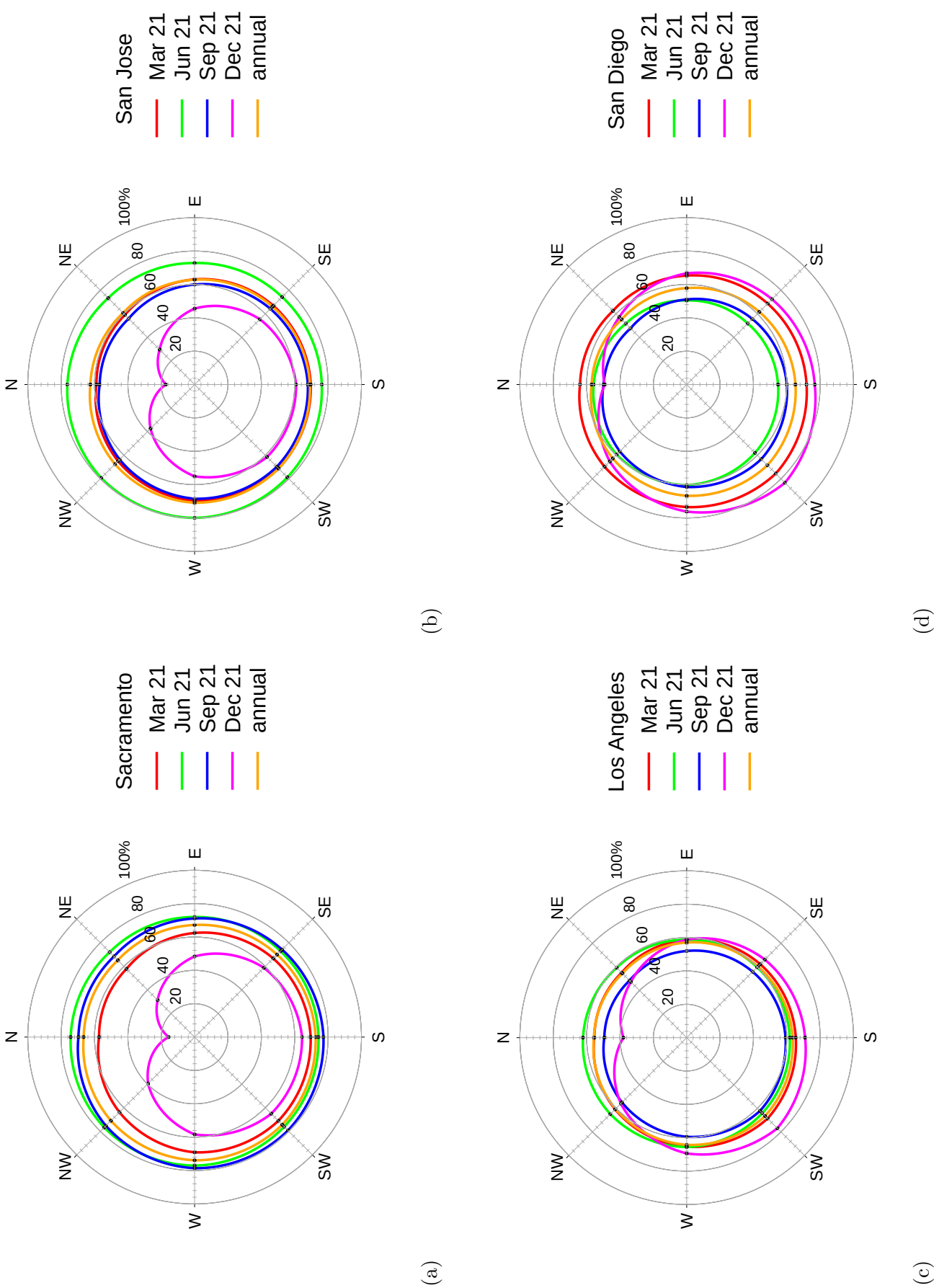

Figure 10: Daily and annual mean direct fractions of global solar irradiation on unshaded 5:12 pitch roofing planes, shown by aspect in (a) Sacramento, (b) San Jose, (c) Los Angeles and (d) San Diego.

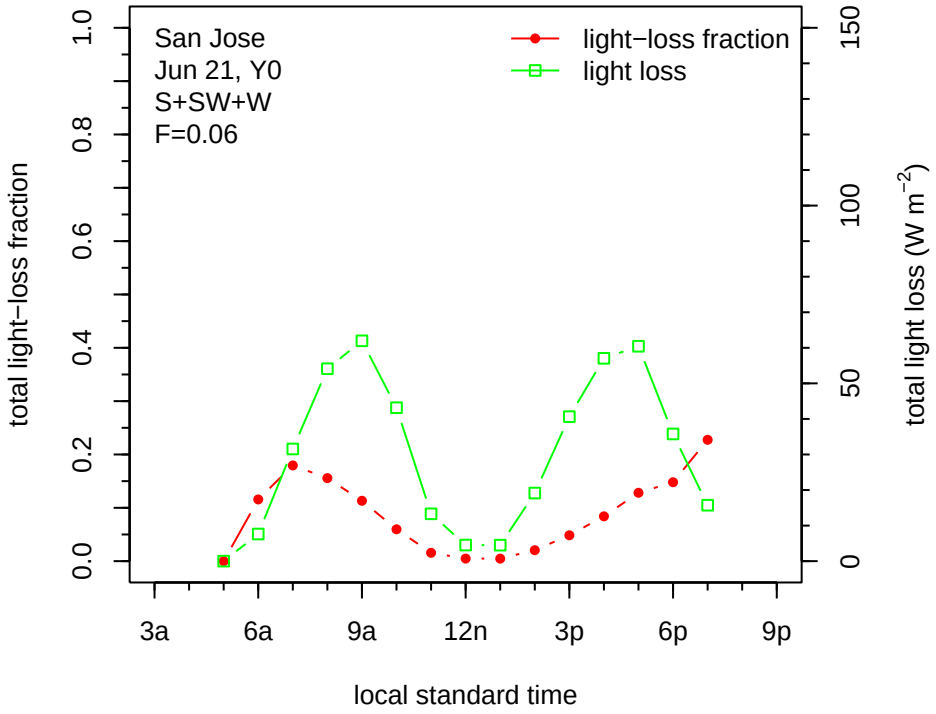

(a)

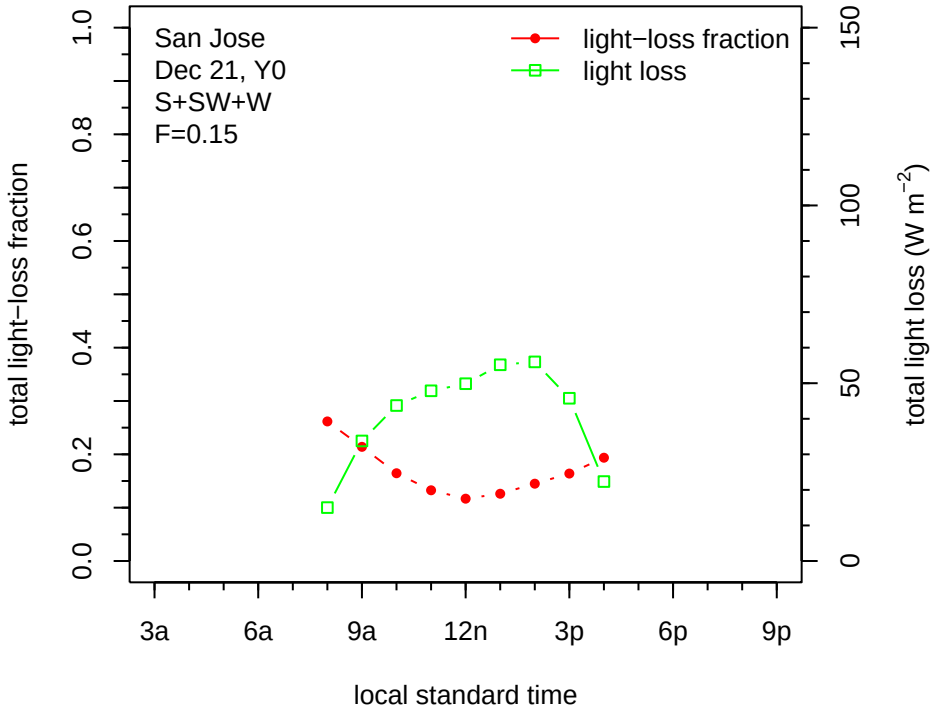

(b)

Figure 11: Year-zero on-hour total light loss fraction and total light-loss of S+SW+W roofing planes in San Jose on (a) June 21 (the summer solstice) and (b) December 21 (the winter solstice). Also shown is the daily total light loss fraction F.

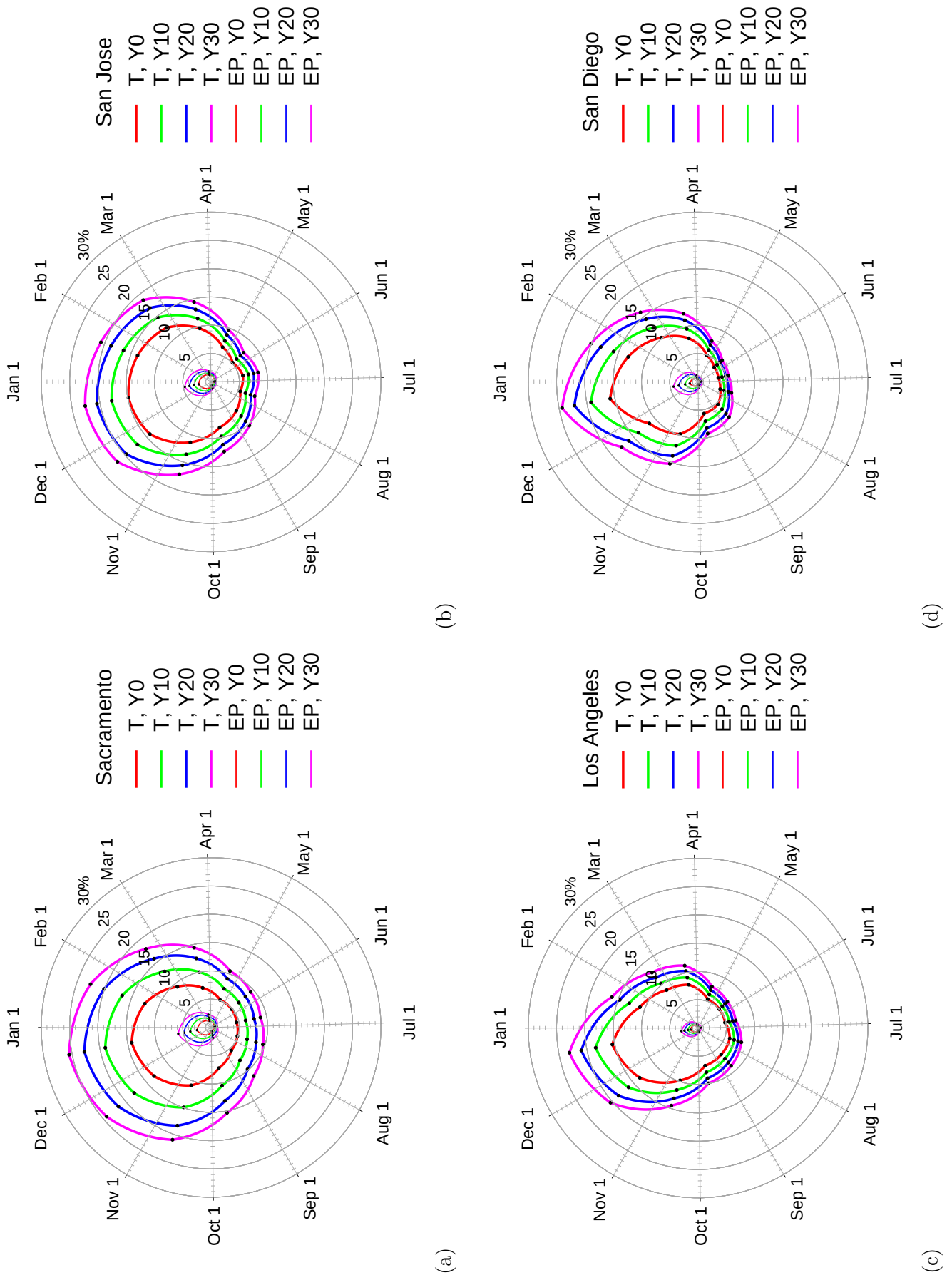

Figure 12: Daily total (T) and extraparcel (EP) light-loss fractions of S+SW+W planes by year (Y) in (a) Sacramento, (b) San Jose, (c) Los Angeles and (d) San Diego.

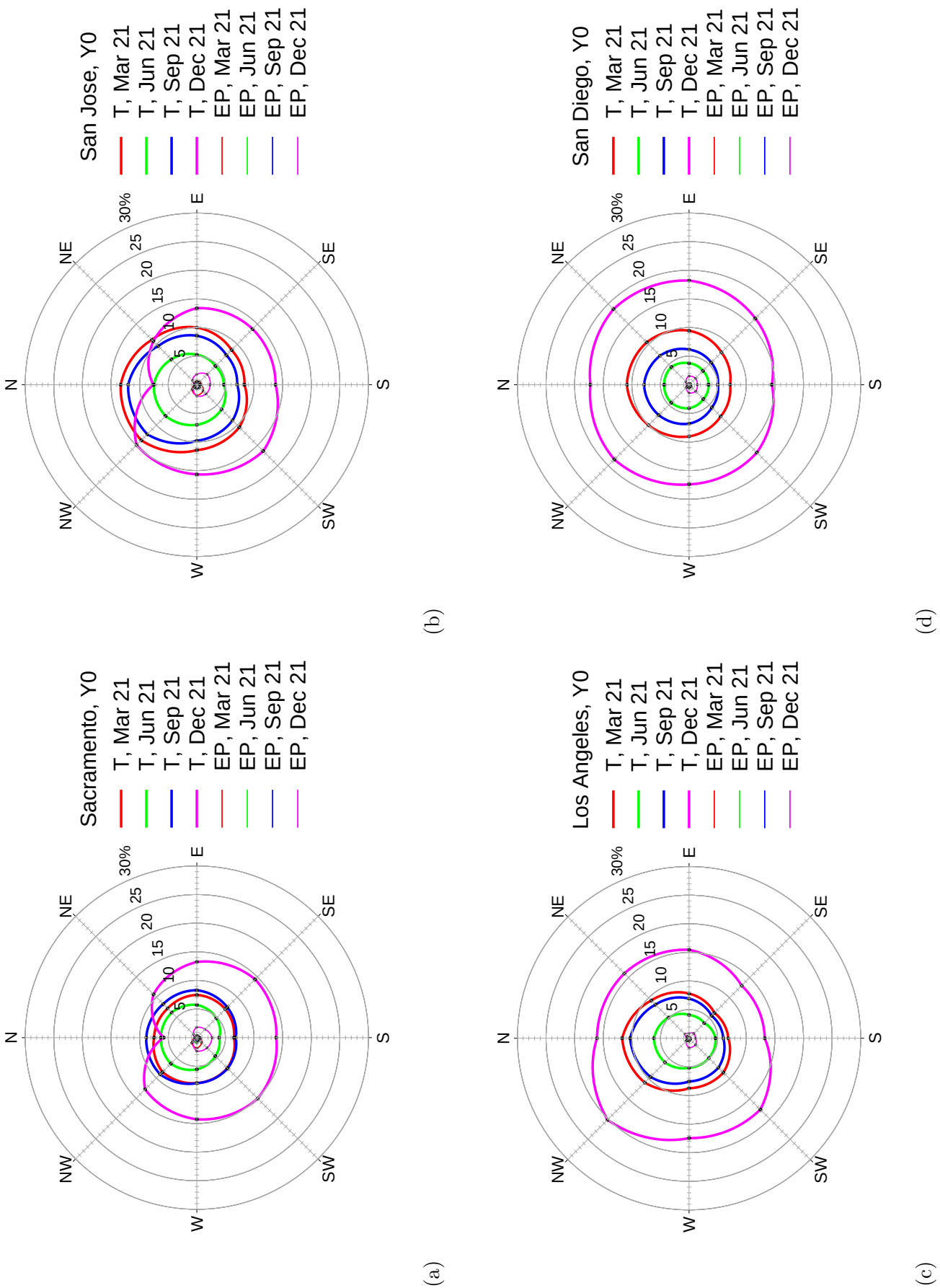

Figure 13: Daily total (T) and extraparcel (EP) light-loss fractions in year 0 by aspect in (a) Sacramento, (b) San Jose, (c) Los Angeles and (d) San Diego.

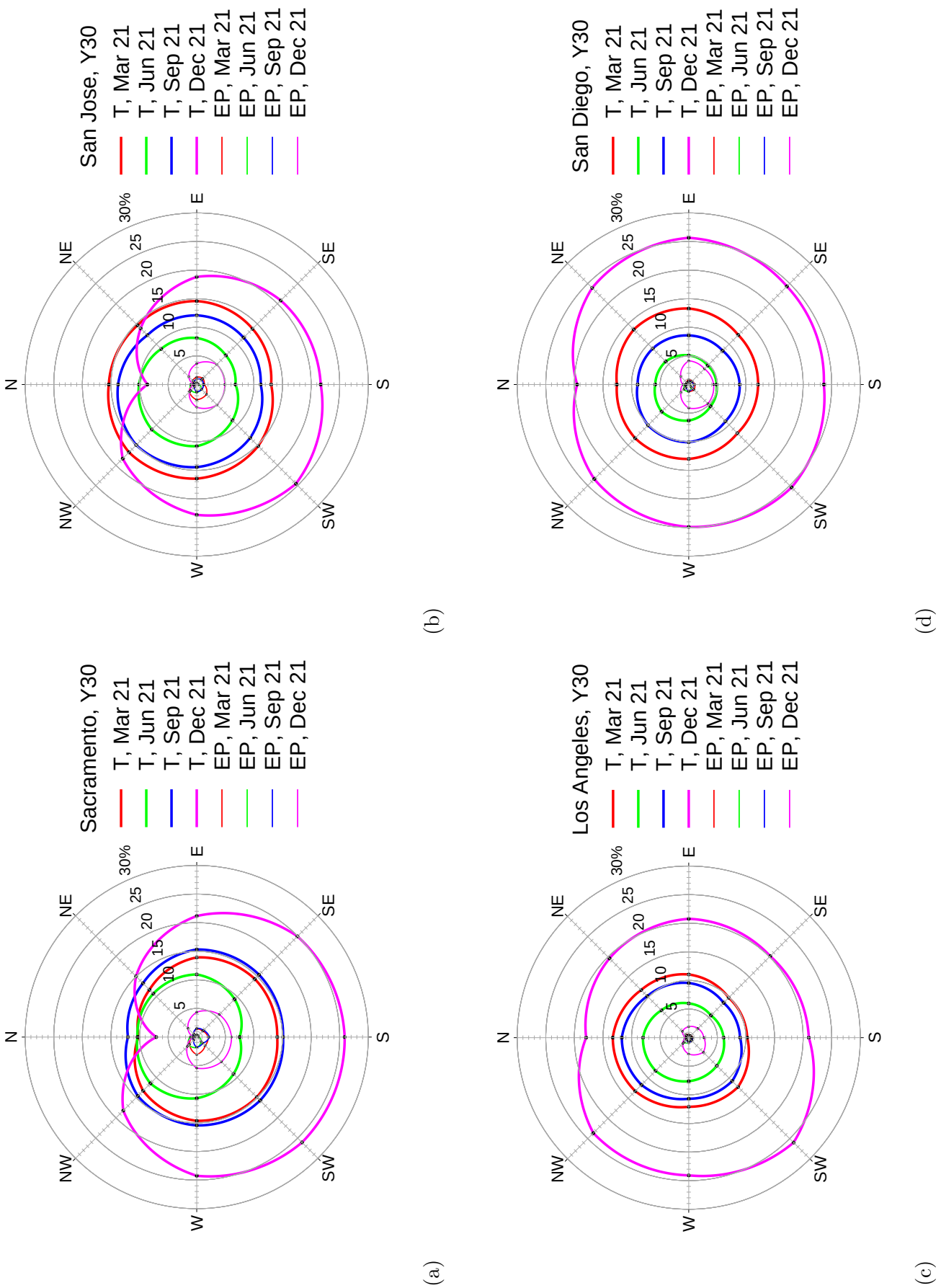

Figure 14: Daily total (T) and extraparcel (EP) light-loss fractions in year 30 by aspect and day in (a) Sacramento, (b) San Jose, (c) Los Angeles and (d) San Diego.

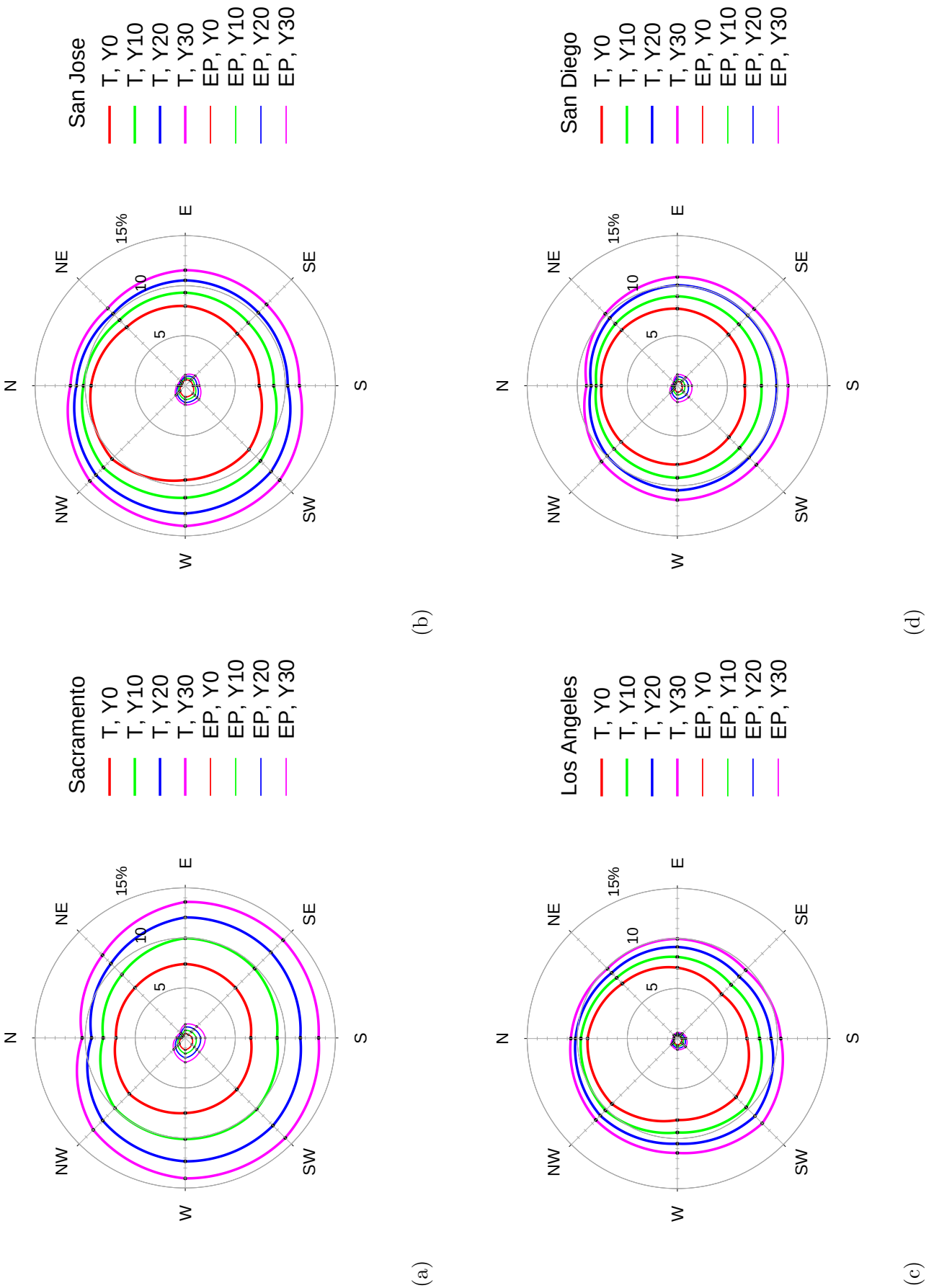

Figure 15: Annual total (T) and extraparcel (EP) light-loss fractions of planes by year (Y) and aspect in (a) Sacramento, (b) San Jose, (c) Los Angeles and (d) San Diego.

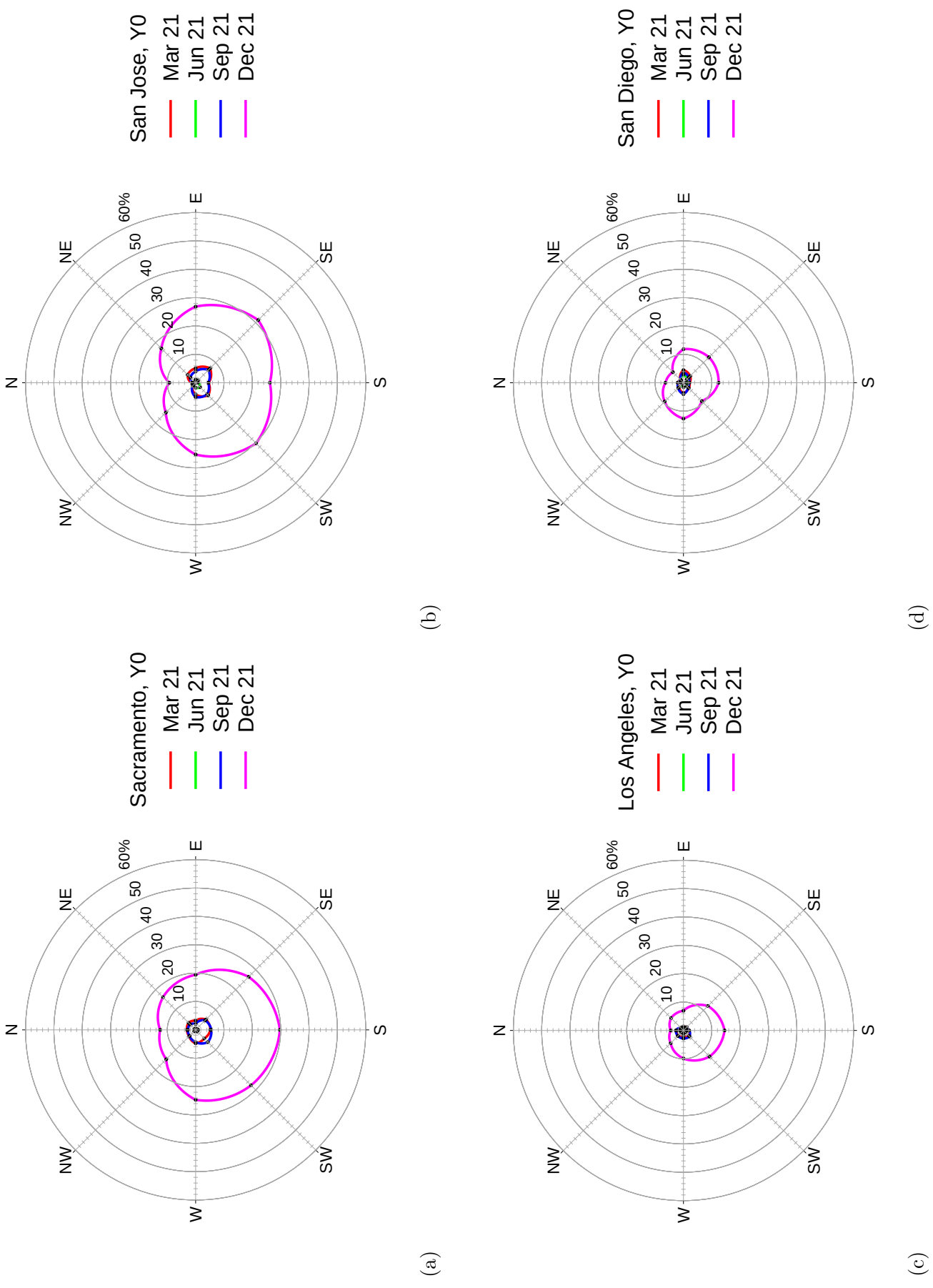

Figure 16: Fraction of planes in solar access violation in year 0 by aspect and day in (a) Sacramento, (b) San Jose, (c) Los Angeles and (d) San Diego.

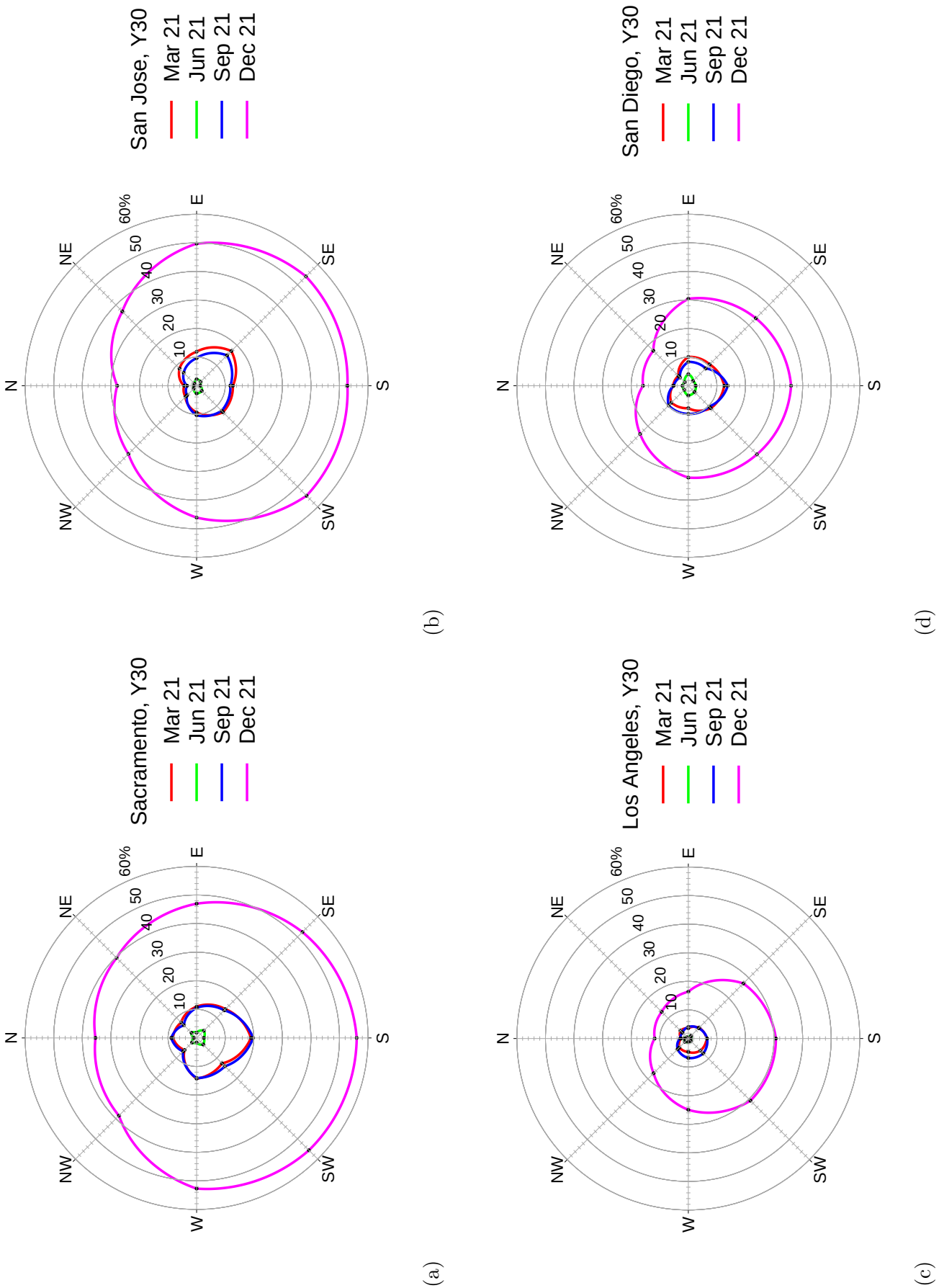

Figure 17: Fraction of planes in solar access violation in year 30 by aspect and day in (a) Sacramento, (b) San Jose, (c) Los Angeles and (d) San Diego.